Lead Telluride Quantum Dot Solar Cells Displaying External Quantum Efficiencies Exceeding 120%

Marcus L. Böhm,[†] Tom C. Jellicoe, [†] Maxim Tabachnyk, [†] Nathaniel J. L. K. Davis, [†] Florencia Wisnivesky-Rocca-Rivarola,[‡] Caterina Ducati, [‡] Bruno Ehrler,[#] Artem A. Bakulin[†] and Neil C. Greenham[†,]*

[†] *Cavendish Laboratory, University of Cambridge, J. J. Thomson Avenue, Cambridge, CB3 0HE, UK*

[‡] *Department of Materials Science and Metallurgy, University of Cambridge, 27 Charles Babbage Road, Cambridge, CB3 0FS, UK*

[#] *Center for Nanophotonics, FOM Institute AMOLF, Science Park 104, 1098 XG, Amsterdam, The Netherlands*

[*] *Corresponding author, ncg11@cam.ac.uk*

- *Supporting Information* –

S1 – Absorbance and Transmission Spectra and Electron Microscopy

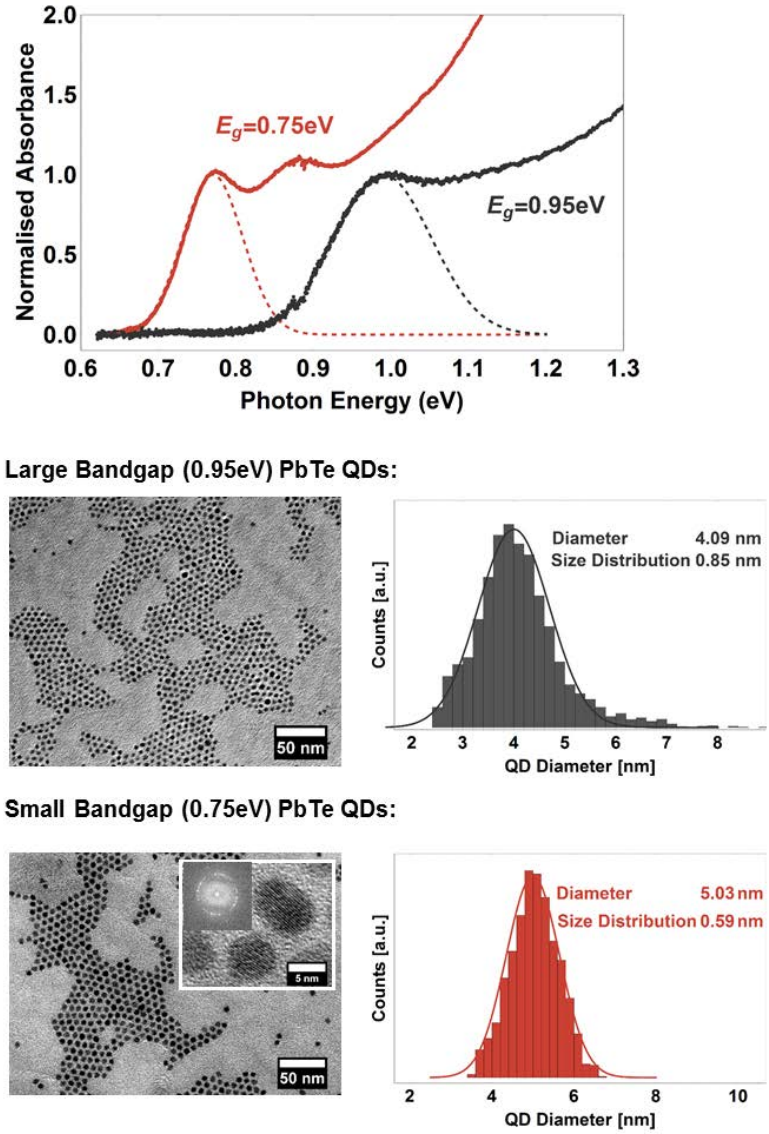

Figure S1: Absorbance and transmission electron microscopy (TEM) spectra of two sizes of as-synthesised PbTe CQDs.

The size distribution (SD) was determined optically by fitting a Gaussian function to the first excitonic peak. For an independent analysis via TEM a histogram of the diameter distribution of more than 3000 individual particles was produced using Image J (http://imagej.nih.gov/ij/). The QD size distribution was then derived via the standard deviation of the histogram produced (see Table S1).

Table S1: Size distribution of PbTe quantum dots as determined by absorbance spectroscopy and TEM.

Size Distribution	Absorbance [%]	TEM [%]
E_g = 0.95 eV	15.9	20.7
E_g = 0.75 eV	11.6	11.7

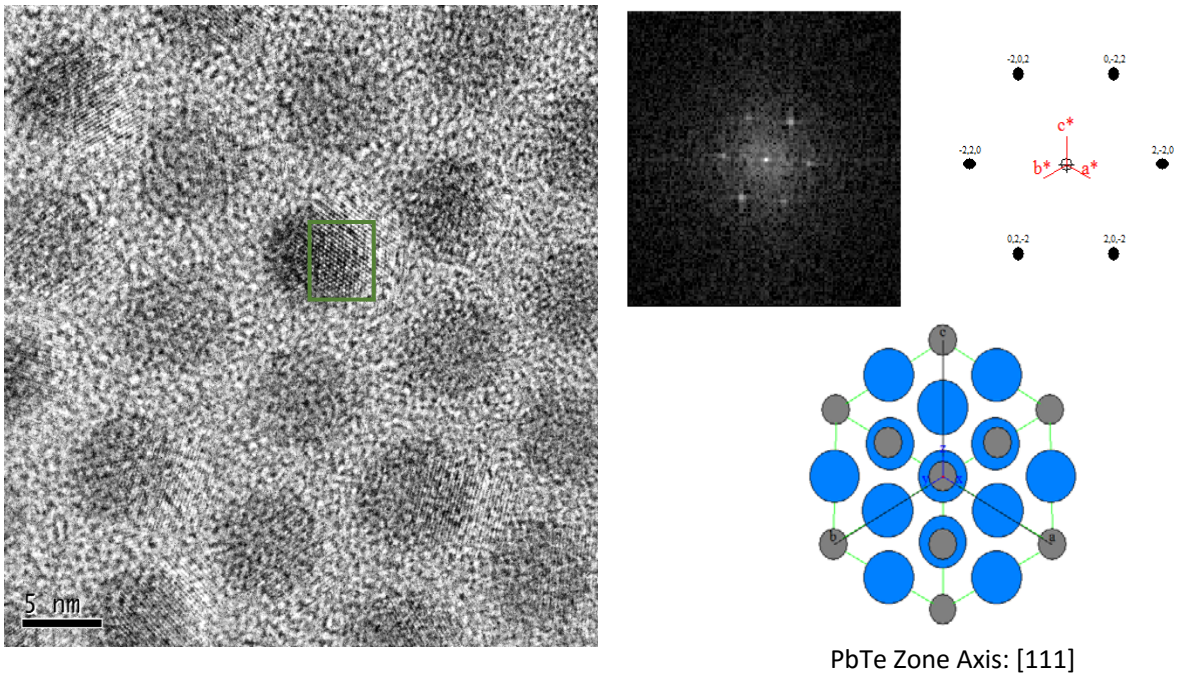

Figure S2: HR TEM on small bandgap PbTe QDs (E_g = 0.75 eV). To identify the PbTe [1 1 1] zone axis the fast Fourier transform (FFT) of the indicated area in the HR TEM image was used.

S2 – Ultraviolet photoelectron spectroscopy (UPS) on PbTe QDs

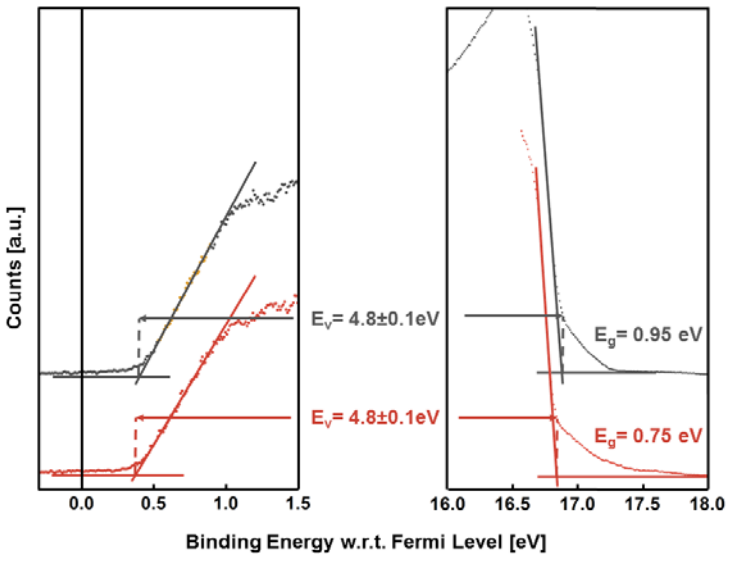

Figure S3: Ultraviolet photoelectron spectroscopy (UPS) on PbTe CQDs of the bandgap 0.75 eV (red) and 0.95 eV (gray).

S3 – Photovoltaic performance of small- and large-bandgap PbTe QDs if TiO_2 is employed as an electron-collecting layer

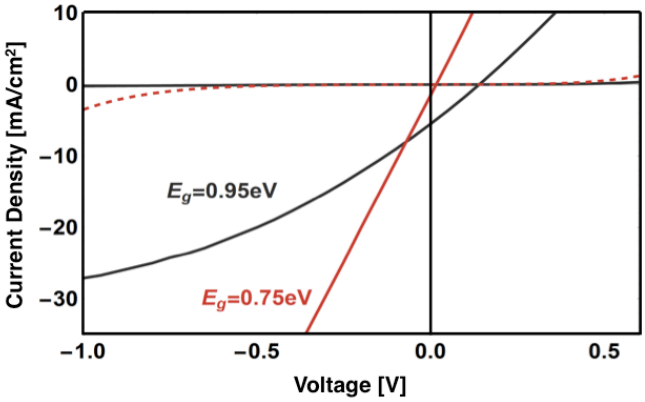

Figure S4: IV curves of PbTe QD devices employing TiO_2 as electron extraction layer

S4 – Photovoltaic performance of PbTe QDs if ZnO is employed as an electron-collecting layer

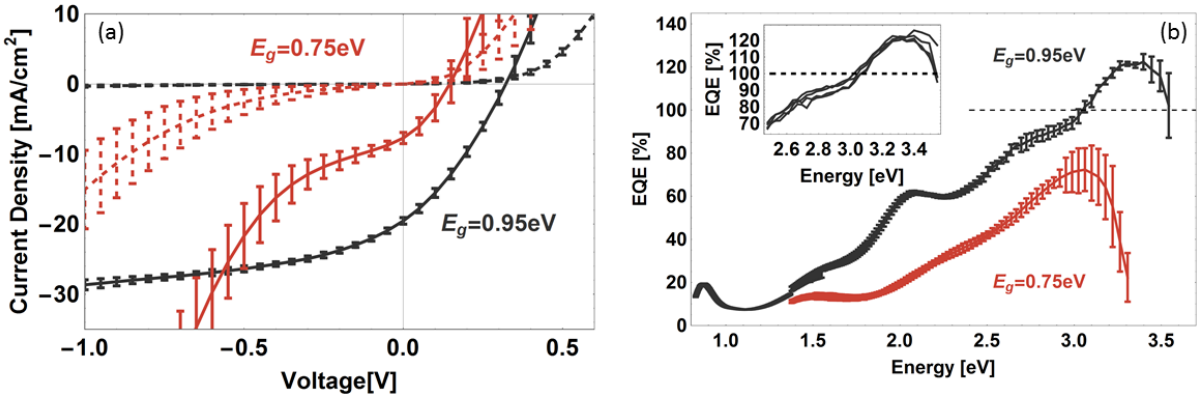

Figure S5: (a) Current-voltage and (b) external quantum efficiency (EQE) of PbTe QD-based solar cells employing ZnO as the electron-extracting layer. The irregularity in the EQE around 1.5 eV arises from different UV exposure times leading to a different photoconductivity in the ZnO (see experimental details for further explanation).

S5 – Integrated EQE

The photocurrent under short-circuit conditions was reconstructed by multiplying the EQE at each wavelength with the corresponding incident power under AM1.5 irradiation. Integration over all wavelengths produced a short-circuit current (J_{SC}) of 18.4±0.6 mA/cm^2. The average measured J_{SC} is 17.8 ± 0.3 mA/cm^2, which is ca. 3 % lower than the calculated value.

S6 – EQE measurements under tuneable background illumination

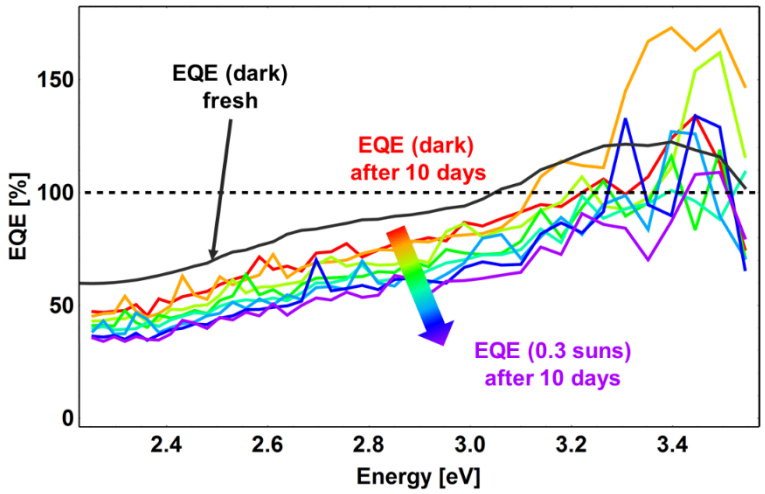

Figure S6: White light bias dependent EQE measurements in the high-energy region of the solar spectrum.

We note that the EQE measurements performed under various white light background (WLB) illuminations were performed 10 days after the EQE measurement conducted without a WLB (see Figure 1(c) of the main text) and show a lower photocurrent under similar measurement conditions. We explain this phenomenon with QD surface oxidation effects[1,2] which are likely to reduce the extractable photocurrent under short-circuit conditions (see Figure S6).

The lower quantum efficiency at higher white-light intensity is indicative of a carrier-density dependent charge recombination. Transient photovoltage measurements under different white light intensities (see Figure S7) confirm this.

S7 – Transient photovoltage decay measurements under tuneable back ground illumination for devices consisting of PbTe QDs.

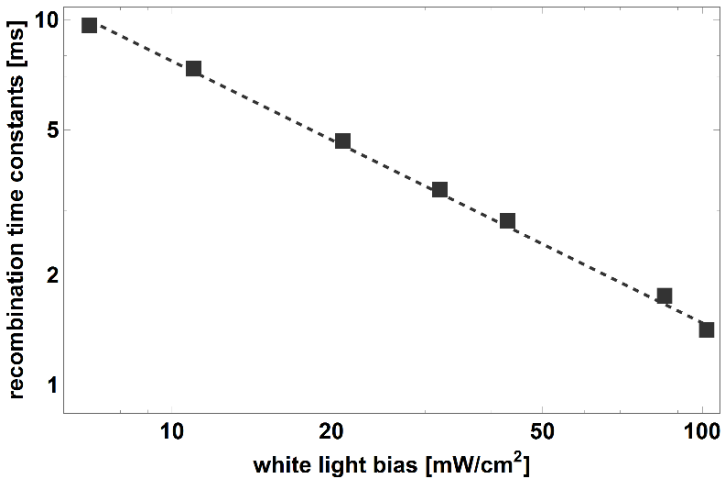

Figure S7: White light bias dependence of the transient photovoltage decay pf PbTe-based photovoltaic devices.

Transient photovoltage measurements were performed according to our previously published experimental method.[3] Briefly, we used a 525 nm green LED (Kingbright, L-7104VGC-H) as the monochromatic, pulsed light source, and a set of six white high-brightness LEDs was used to provide constant background illumination. A set of lenses was used to focus the incident light of both the pulse light source and the background light source onto a single pixel of the device. A Hewlett Packard (HP) 8116A function generator was used to power the LED. The intensity of the background illumination was calibrated by comparing the short-circuit current density (J_{SC}) with the values previously obtained from the solar simulator. Open-circuit voltage transients were recorded by connecting the device under test in series with an Agilent DSO6052A digital oscilloscope with input impedance of 1MΩ.

S8 – Calibration curves for the Si and Ge diodes used

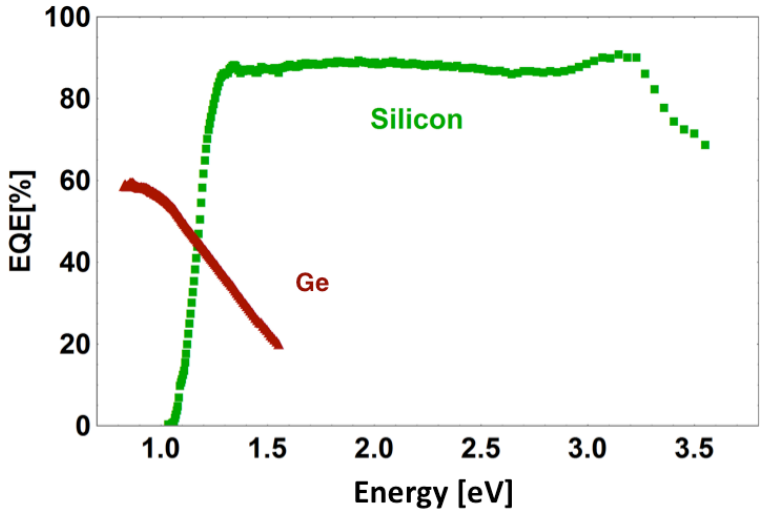

Figure S8: Calibration curves for the Si and Ge diodes employed for reflectivity measurements.

S9 – *n* and *k* values for each device layer as determined by ellipsometry

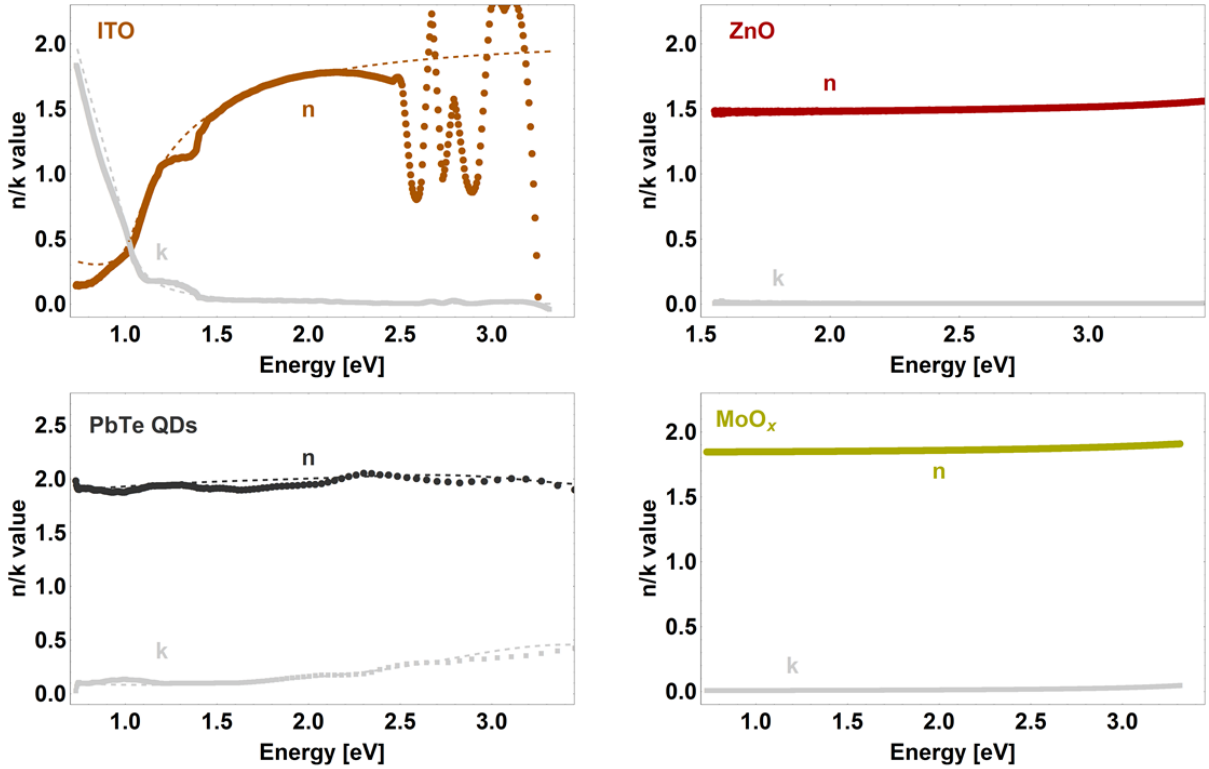

Figure S9: Refractive index n and the exctinction coefficient k of ITO, ZnO, PbTe QDs (E_g=0.95 eV) and MoO_x. The curves for ITO, ZnO and MoO_x have been drawn from previous work.[4] The point-by-point fit is shown as unconnected dots and the applied model is presented as dashed lines. n and k values for Ag have been taken from the literature.[5]

S10 – Transient absorption

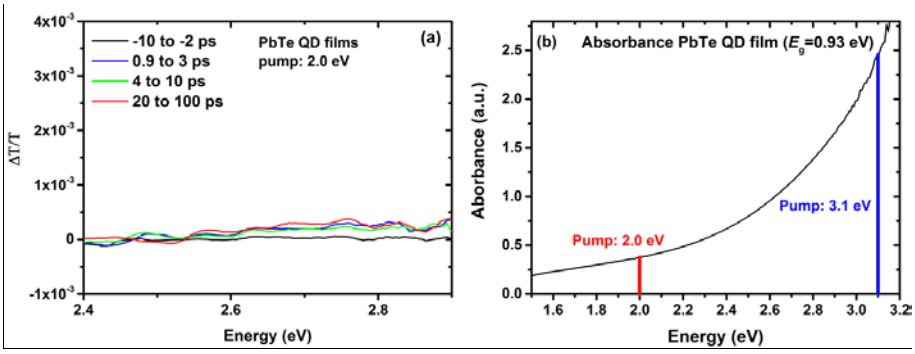

Figure S10: (a) Raw transient absorption spectrum of a PbTe QD film (E_g=0.93 eV) after an initial pump excitation at 2.0 eV (60μJ/cm^2).(b) Absorbance profile of the PbTe QD film in the spectral region of the two pump excitation energies.

In Figure S10(a) we show the transient absorption spectrum after an excitation at 2.0 eV, which is below the ground state bleach (GSB) energy observed in Figure 4(a) of the main text. In agreement with previous transient absorption measurements on PbS and PbSe QDs[6] we find no notable GSB signal in this region. We note that the excitation density generated by the 2.0eV pump is significantly smaller than for the 3.1eV pump. This phenomenon arises due to three effects: First, the PbTe QD sample absorbs ca. 6.0 times less at 2.0 eV compared to 3.1eV (see Figure S10(b)); second, we doubled the pump fluence for the lower pump excitation; and third, the generated photon flux at 2.0 eV is ca. 1.5 times higher than at 3.1 eV. Considering all three effects we estimate the excitation density generated by the 2.0eV pump to be a factor of 1.9 times smaller than for the 3.1eV pump

S11 – Long-time Pump-Push Photocurrent

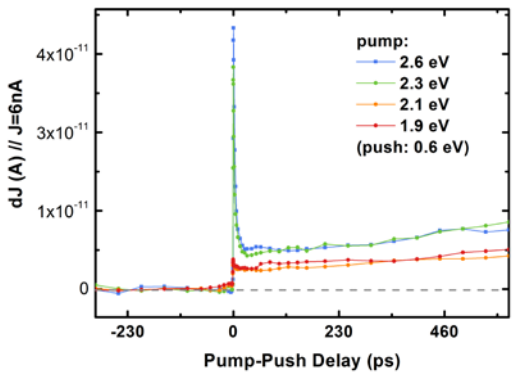

Figure S11: Photocurrent response as a function of (long) time delay between pump and push pulse. The fluence of the pump excitation has been adjusted to produce 5 nA for each excitation energy. The transients were corrected for the response at negative delay times. The transients clearly contain two components where the early dynamics can be interpreted in the framework of MEG. The long-lived signal including the growing component at >100 ps delay have been previously assigned to the delayed charge-transport-assisted trapping of photogenerated charge carriers.[7]

S12 – Kinetics of the pump-push-photocurrent experiment

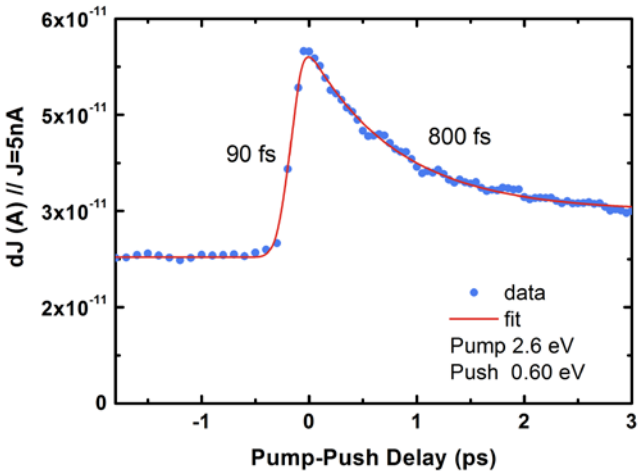

Figure S12: Photocurrent response as a function of time delay between pump and push pulse. The photocurrent due to the pump pulse only was 5nA. The transient has not been corrected for the response at negative delay times. The red line is a fit to the data using an exponential 800fs decay function convolved with the 80fs Gaussian response function of the setup.

Bibliography:

(1) Bae, W. K.; Joo, J.; Padilha, L. a; Won, J.; Lee, D. C.; Lin, Q.; Koh, W.; Luo, H.; Klimov, V. I.; Pietryga, J. M. *J. Am. Chem. Soc.* **2012**, *134*, 20160–20168.

(2) Bode, D.; Levinstein, H. *Phys. Rev.* **1954**, *96*, 259.

(3) Böhm, M. L.; Kist, R. J. P.; Morgenstern, F. S. F.; Ehrler, B.; Zarra, S.; Kumar, A.; Vaynzof, Y.; Greenham, N. C. *Adv. Energy Mater.* **2014**, 1400139.

(4) Davis, N. J. L. K.; Böhm, M. L.; Tabachnyk, M.; Wisnivesky-Rocca-Rivarola, F.; Jellicoe, T. C.; Ducati, C.; Ehrler, B.; Greenham, N. C. *Nat. Commun., in press.*

(5) Winsemius, P.; Kampen, F. F. Van; Lengkeek, H. P.; Went, C. G. Van. *J. Phys. F Met. Phys.* **2001**, *6*, 1583–1606.

(6) Geiregat, P.; Delerue, C.; Justo, Y.; Aerts, M.; Spoor, F.; Thourhout, D. Van; Siebbeles, L. D. A.; Allan, G.; Houtepen, A. J.; Hens, Z. *ACS Nano* **2015**, *9*, 778–788.

(7) Bakulin, A. A.; Neutzner, S.; Bakker, H. J.; Ottaviani, L.; Barakel, D.; Chen, Z. *ACS Nano* **2013**, *7*, 8771.